第34卷 第2期 焊 接 学 报 Vol. 34 No. 2
2013年2月 TRANSACTIONS OF THE CHINA WELDING INSTITUTION February 2013

细径铜丝超声键合焊点高温存储可靠性分析

杭春进[1,2]， 田艳红[1]， 王春青[1]， 赵九蓬[2]
(1. 哈尔滨工业大学 现代焊接生产技术国家重点实验室，哈尔滨 150001；
2. 哈尔滨工业大学 化学工程与技术学院，哈尔滨 150001)


杭春进

摘 要：对塑封后的20 μm细径铜丝超声键合焊点进行了高温存储可靠性研究. 采用SEM观察了老化后键合焊点界面微观组织及金属间化合物，采用EDS对反应物的成分进行了分析. 结果表明，200 ℃老化9天或250 ℃老化9 h，键合焊点界面生成了大量Cu-Al金属间化合物，并出现可见的微裂纹和Kirkendall孔洞；250 ℃老化16 h后，环氧塑封料中微量的Sb元素与铜球焊点发生反应，生成以Cu_3Sb为主的反应物；当老化时间超过49 h，铜丝破碎，铜键合焊点产生严重腐蚀. 250 ℃老化超过24 h或300 ℃老化超过4 h会发生银迁移现象.

关键词：细径铜丝；高温存储；金属间化合物；可靠性；银迁移
中图分类号：TG409 **文献标识码**：A **文章编号**：0253－360X(2013)02－0013－04

0 序 言

随着微电子器件封装技术向细引脚间距化方向发展，细直径铜丝呈现出了替代金丝的趋势. 即使直径非常细的铜丝仍能够保持键合结构的刚度，能够很好地避免丝摆等问题的出现[1－4]. 通常铜丝仍然与传统的铝焊盘进行键合. 对Cu/Al和Au/Al的界面反应进行比较，结果发现Cu/Al界面金属间化合物(IMC)的生长速度要比Au/Al慢一倍以上，而且在150～200 ℃的老化温度范围内界面上仅会形成$CuAl_2$和CuAl，其中脆性的$CuAl_2$会引起接头强度的轻微下降[5－7]. 此外塑封后的键合结构在进行可靠性试验时，除了键合金属界面会不断地生成金属间化合物外，来自于塑封料(EMC)内的卤族元素和Cl^-也会与键合结构发生反应，导致器件失效[8－11]. 然而关于Cu/Al键合结构与EMC之间的反应及失效机理尚不清楚.

文中采用高温存储试验对采用直径为20 μm的铜丝所获得的Cu/Al超声引线键合点在塑封状态下的可靠性进行了研究，考察了界面IMC与裂纹的形成和演变行为，同时研究了从塑封料中释放出来的锑与铜在高温存储时发生的反应.

收稿日期：2011－12－28
基金项目：国家自然科学基金资助项目(50705021)；中央高校基本科研业务费专项资金资助项目(HIT. NSRIF. 2010/20)

1 试验方法

文中以小外形晶体管(small outline transistor，SOT)作为研究对象，采用20 μm铜丝进行了超声丝球键合，并采用通用的商业EMC对键合后的SOT进行塑封，结构如图1所示. 铜丝纯度为99.99%(质量分数)，具有7%～13%的断后伸长率. 铜球焊点对应的铝焊盘厚度为3 μm，楔焊点键合在镀银引线框架上，键合机为ASM Eagle 60. 对于球形焊点采用的超声功率为65 mW，键合压力为0.3 N，键合时间为6 ms，键合温度为220 ℃. 楔焊点的键合工艺为超声功率85 mW，键合压力0.5 N，键合时间10 ms. 为防止铜球形成过程中发生氧化，采用了95% N_2 + 5% H_2 的保护气体，气体流速为0.6 L/min.

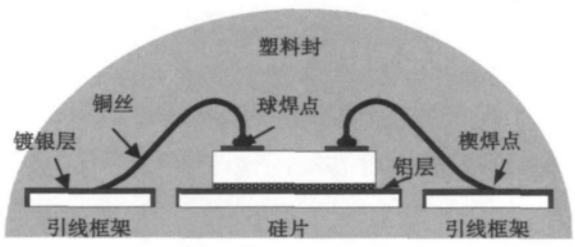

图1 塑封状态下小外形晶体管结构示意图

Fig. 1 Schematic drawing of SOT device after encapsulation

塑封后的 SOT 首先进行电气功能测试，测试合格的 SOT 进行高温存储试验. 试验分别采用了 200 ℃，最长保温 25 天；250 ℃，最长保温 49 h；300 ℃，最长保温 9 h.

老化后的 SOT 在空气中自然冷却，之后采用环氧树脂进行灌封，制成分析试样. 采用 SiC 砂纸进行打磨，并依次采用直径为 3，1，0.5 μm 的金刚石悬浮液进行抛光. 采用 HITACHI S-4700 扫描电镜(SEM)进行键合点截面形貌观察，同时采用 X 射线能谱仪(EDS)对界面反应物进行成分分析.

2 试验结果

2.1 200 ℃ 恒温老化

图 2 给出了 200 ℃条件下经过不同老化时间后 Cu/Al 键合焊点界面的 SEM 形貌.

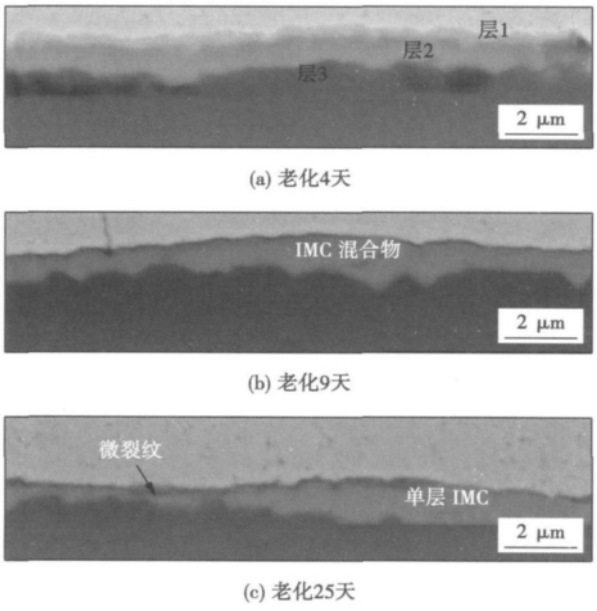

图 2 200 ℃下不同老化时间 Cu/Al 键合焊点界面 SEM 形貌

Fig. 2 SEM pictures of Cu/Al bond cross-sections at 200 ℃ with different aging time

可见经过 4 天的老化，焊点界面上形成了连续的 IMC 层，从反应层呈现不同的颜色推测，反应层主要由 3 种类型的 IMC 构成，如图 2a 所示. 当老化时间达到 9 天，IMC 层和铜焊盘之间形成了连续的裂纹，从而导致铜球从铝焊盘上脱离，电气连接完全失效，如图 2b 所示. 裂纹的形成同时也导致了 Cu 原子扩散通道的断开，随着 Al 原子不断地扩散进入 IMC 层，IMC 逐渐转变成单层 IMC，如图 2c 所示. Hang 等人[12]的研究结果表明，图 2b 中的 IMC 从铜侧至铝侧分别为 Cu_9Al_4，CuAl 和 $CuAl_2$. 将铜球焊点通过剪切推掉，对断面进行 EDS 分析，结果见图 3. 可见图 2c 中的 IMC 相的 Cu/Al 原子比约为 1∶2. 因此该 IMC 是 $CuAl_2$，这与文献[3]的结论一致.

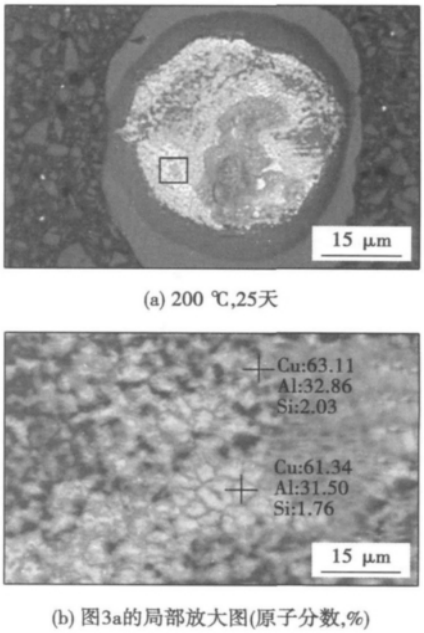

图 3 铜球键合界面 Cu-Al 金属间化合物 EDS 分析结果

Fig. 3 EDS results of IMCs at Cu-Al interface

2.2 250 ℃恒温老化

图 4 为 250 ℃、不同老化条件下的 Cu/Al 焊点界面 SEM 形貌. 仅经过 1 h 老化，Cu/Al 界面就会快速生成 Cu/Al IMC. 当老化时间增加至 4 h，界面处就会形成大约 0.5 μm 厚的 IMC 层，如图 4b 所示. 老化时间为 9 h，界面处形成柯肯达尔孔洞和不连续的裂纹，此时 IMC 层的厚度大约为 1 μm，如图 4c所示.

图 5 所示为 250 ℃不同老化时间条件下塑封料与铜球焊点之间的反应. 经过 25 h 的老化，铜球与铝焊盘完全分离，EMC 中的活性元素与铜球发生反应，生成的新物质将铜球完全包裹，在白色反应层与铜球间形成了可见的裂纹，如图 5a 所示. 随着老化时间的延长，反应延伸到铜球内，铜球的圆形结构开始变得疏散，在铜球边缘形成了大量微孔洞，大量反应物在铜球表面形成，如图 5b 所示. 这些脆性的反应物非常容易发生破碎. EDS 分析结果显示白色反应物中锑原子分数为 22% ~23%. 根据 Cu-Sb 二元合金相图[13]，白色相可能为 Cu_3Sb. Sb 元素来自于 EMC 中的 Sb_2O_3，其分解阈值温度大约在 200 ~250 ℃之间. 低于 200 ℃时，Sb_2O_3 难以分解. 经 250 ℃

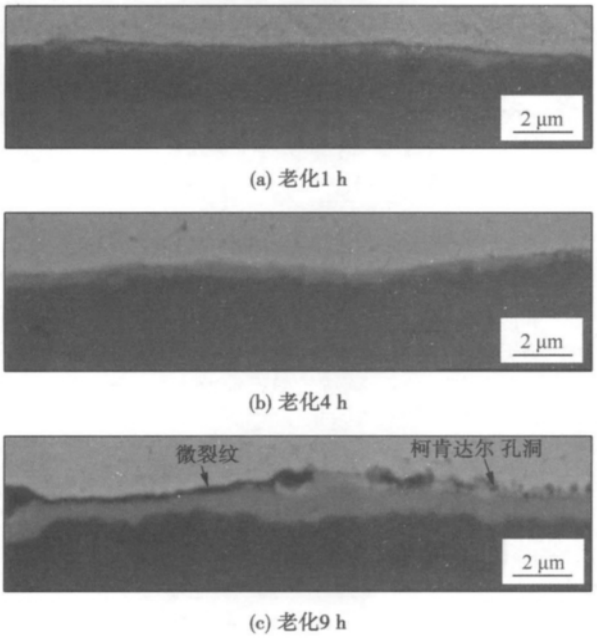

图 4　250 ℃下不同老化时间 Cu/Al 键合焊点界面 SEM 形貌
Fig. 4　Cu/Al bond cross-sections at 250 ℃ with different aging time

老化时间超过 24 h 后，分解出来的 Sb 元素将与铜发生剧烈反应. 同时引线框架上的银开始发生迁移. 图 6a 显示部分银已经从银层表面迁移到了塑封料中. 迁移的路径呈现明显的树枝状. 当老化时间达到 96 h，已经有大量的银穿过塑封料迁移到了铜球的表面，如图 6b 所示.

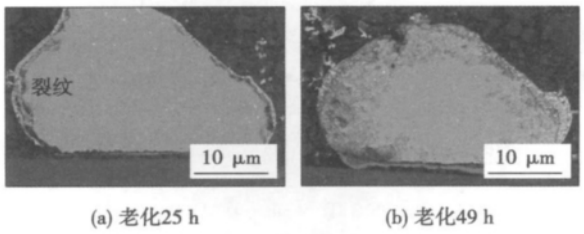

图 5　250 ℃不同老化时间条件下 EMC 与铜球焊点之间的反应
Fig. 5　Cu bonds aged at 250 ℃ with different aging time

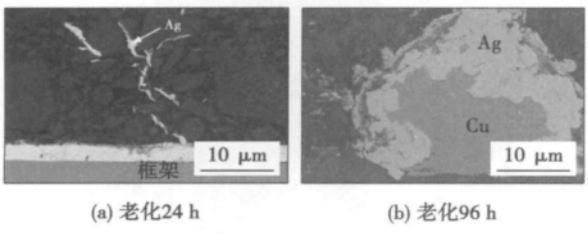

图 6　250 ℃不同老化时间条件下银迁移现象
Fig. 6　Ag migration at 250 ℃ with different aging time

2.3　300 ℃恒温老化

当老化温度升高到 300 ℃时，树脂基塑封料与铜引线键合样品的反应更加剧烈. 老化 1 h 后铜丝弯曲部位的内侧形成了多个点蚀，如图 7a 所示. 老化 4 h 之后，球颈部位的铜丝几乎全部反应掉，铜球表面被反应物包围，铜球内部沿晶粒边界破碎，如图 7b 所示.

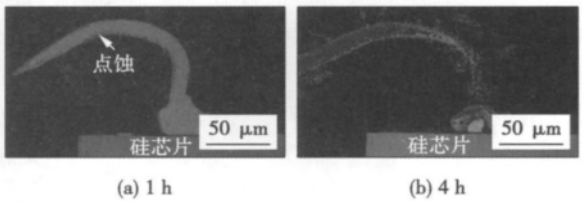

图 7　300 ℃不同老化时间条件下铜焊点界面
Fig. 7　SEM of Cu bonds aged at 300 ℃

与此同时，银迁移现象也同步发生，如图 8a 所示. 此时银不仅向塑封料中迁移，且沿着硅芯片侧面向上迁移. 并且部分银向硅芯片上表面迁移，如图 8b 所示. 铜丝内部也发生明显变化，大量银迁移到了铜丝内部，与浅灰色的 Cu/Sb 相共同取代了铜丝原来的位置，如图 8c 所示.

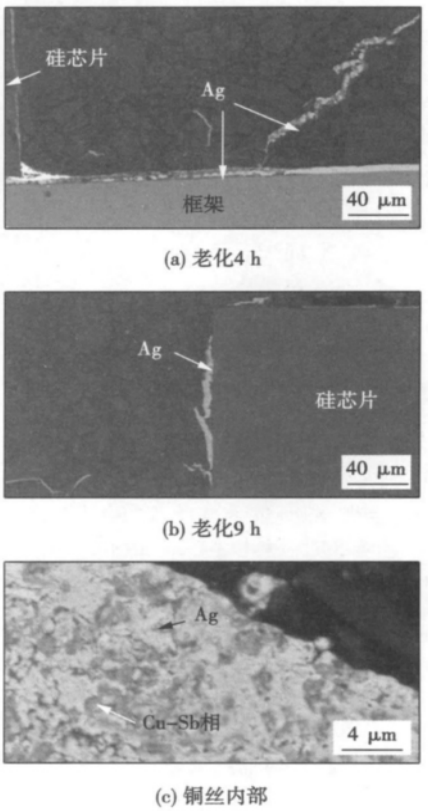

图 8　300 ℃下银迁移现象
Fig. 8　Ag migration at 300 ℃

从试验结果可以发现银迁移现象有以下几个特征: 在温度高于一定值的(250 ℃) 条件下才发生; 迁移方向是从银至铜; 迁移沿着塑封料与填充料和硅芯片之间的界面进行的,且呈现为放电状的形状,类似于电化学迁移行为. 铜,银的标准电极电位分别为 +0. 337 V 与 +0. 799 1 V,二者之间电位差为 0. 462 1 V; 楔焊点直接连通铜丝与银层; 高温环境中线膨胀系数相差较大的塑封料与硅块之间产生很大的界面应力并导致微裂纹. 而塑封料中的卤化物、Cl^-等小分子物质向裂纹聚集并形成类似于溶液的混合物. 当微裂纹相互连通时,铜丝与银层之间形成了"溶液"通道,构成了"原电池"结构. 阳极银层不断与微裂纹中的物质发生反应生成 Ag^+, Ag^+在静电场作用下不断地向阴极铜丝运动,形成迁移,最终部分 Ag^+到达铜表面,与电子结合后沉积到铜的表面.

3 结 论

(1) 200 ℃下存储的键合焊点,其 Cu/Al 界面发生扩散反应. 1 天后,界面出现由二层 IMC 层构成的反应层. 随着保温时间的延长,反应层演变为三层 IMC 结构. 9 天后反应层与铜球之间形成连续裂纹,反应层变为单层 IMC 结构,该单层 IMC 为 $CuAl_2$.

(2) 250 ℃条件下,锑会从 EMC 中释放出来与铜焊点发生反应,并生成以 Cu_3Sb 为主的反应物. 随着存储时间的延长,锑会持续与铜球发生反应,最终导致键合结构碎裂.

(3) 250 ℃条件下存储 24 h 后,或 300 ℃条件下存储 4 h 后,出现银向铜丝和铜球方向的迁移现象.

参考文献:

[1] Tian Yanhong, Yang Dongsheng, Wang Chunqing. Optimization on parameters of electronic flame off process of ball bondswith fine diameter copperwire [J]. Transactions of the China Welding Institution, 2011, 32(1): 41 - 44.

[2] Murali S, Srikanth N, Wong Y. Fundamentals of thermo-sonic copper wire bonding in microelectronics packaging [J]. Journal of Material Science, 2007, 42: 615 - 623.

[3] Murali S, Srikanth N, Vath III C J. An evaluation of gold and copper wire bonds on shear and pull testing [J]. Journal of Electronic Packaging, 2006, 128: 192 - 201.

[4] Jiang Wei, Chang Baohua, Du Dong, *et al*. Influence of wire materials and coating thickness on stress conditions in silicon substrate during copper thermosonic wire bonding [J]. Transactions of the China Welding Institution, 2012, 33(3): 13 - 16.

[5] Kim H J, Lee J Y, Paik K W. Effects of Cu/Al intermetallic compound (IMC) on copper wire and aluminum pad bondability [J]. IEEE Transactions on Components & Packaging Technologies, 2003, 26: 367 - 374.

[6] Murali S, Srikanth N, Vath III C J. An analysis of intermetallics formation of gold and copper ball bonding on thermal aging [J]. Material Research Bulletin, 2003, 38: 637 - 646.

[7] Harman G G. Wire bonding in microelectronics materials processes reliability and yield [M]. New York: McGraw-Hill, 2010.

[8] Lantz L, Pecht M. Ion transport in encapsulants used in microcircuit packaging [J]. IEEE Transaction on Components & Packaging Technologies, 2003, 26(1): 199 - 205.

[9] Oldervoll F, Strisland F. Wire-bond failure mechanisms in plastic encapsulated microcircuits and ceramic hybrids at high temperatures [J]. Microelectronics Reliability, 2004, 44: 1009 - 1015.

[10] Park J, Cha H J, Kim B S. Interfacial degradation mechanism of Au/Al and alloy/Al bonds under high temperature storage Test: Contamination epoxy molding compound, wire and bonding strength [J]. IEEE Transaction on Components & Packaging Technologies, 2007, 30: 731 - 744.

[11] Sharma P, Upadhyayula K, Lantz L. Impact of pre-conditioning voltage bias and temperature on reliability of plastic encapsulated microcircuits [J]. Microelectronics Reliability, 1998, 38(4): 581 - 584.

[12] Hang C J, Wang C Q, Mayer M, *et al*. Growth behavior of Cu/Al intermetallic compounds and cracks in copper ball bonds during isothermal aging [J]. Microelectronics Reliability, 2008, 48: 416 - 424.

[13] Wulff F W, Breach C D, Stephan D. Further characterization of intermetallic growth in copper and gold ball bonds on aluminum metallization [R]. Singapore: Proceedings of Semicon Singapore, 2005.

作者简介: 杭春进,男,1978 年出生,博士,讲师. 主要从事微连接与电子封装方面的研究工作. 发表论文 20 余篇. Email: hangcj@hit.edu.cn

MAIN TOPICS, ABSTRACTS & KEY WORDS

Restoration and characteristic analysis of X-ray images of molten pool during laser deep penetration welding GAO Xiangdong[1], XIANG Junbin[1], Khalid M. HAFEZ[2], Katayama SEIJI[3] (1. School of Electromechanical Engineering, Guangdong University of Technology, Guangzhou 510006, China; 2. Central Metallurgical R & D Institute, Cairo 11435, Egypt; 3. Joining and Welding Research Institute, Osaka University, Osaka 5670047, Japan). pp 1 - 4

Abstract: Owing to a strong ability to go through the objects, the radiography can be used to observe and analyze the formation of a molten pool inside weldments during laser deep penetration welding. The shape of a molten pool and the thermal transfer effect of laser power through keyhole can be monitored and analyzed in real-time. During a high-power fiber laser welding on plate of 304 stainless steel, a high-speed radiography camera was used to capture the molten pool images. These captured X-ray images were degenerated and obscure due to the disturbance and noises from the welding process and radiography devices. An arithmetic to restore and intensify the X-ray images of molten pool was proposed to make the X-ray images more clear and enhance the ability to recognize the characteristics of images. The blind deconvolution method was used to estimate the point spreading function of X-ray image degeneration, which was applied as a parameter to implement the Wiener filtering of X-ray image of a molten pool. Also, the X-ray image of a molten pool was intensified by the grey level transformation, and the dynamic of a molten pool was analyzed. Results showed that the proposed algorithm of image restoration and intensification can improve the quality of X-ray images effectively and make the contour of a molten pool more distinct.

Key words: laser deep penetration welding; X-ray image of molten pool; image degradation; image restoration

Fatigue life prediction of laser-MIG hybrid welded 7075-T6 Al alloy joints WU Shengchuan[1,2], ZHOU Xinmiao[1], ZHANG Weihua[2], YU Xiao[1], XU Xiaobo[1] (1. School of Materials Science and Engineering, Hefei University of Technology, Hefei 230009, China; 2. State Key Laboratory of Traction Power, Southwest Jiaotong University, Chengdu 610031, China). pp 5 - 8

Abstract: Fatigue crack propogation life of laser-MIG hybrid welded 7075-T6 Al alloy thin plate was investigated, and the relation of heat input and elastic modulus was established by experiments. Moreover, the fatigue life was predicted with different heat input. Based on the improved forman equation, an integrated fatigue life model was formulated with the coupling effect of the property difference, threshold of stress intensity factor, driving force of cracking and residual stress of hybrid welded 7075-T6 joints. This novel model was then validated through real fracture propagation, tensile tests and finite element simulation. It has been proved that the predicted fatigue life shows a good agreement with experimental results.

Key words: hybrid laser-MIG welding; high strength aluminum alloys; fatigue life; threshold of stress intensity factor; residual stress

Analysis on welded joint of thick Ti-6Al-4V plate by magnetically controlled narrow-gap TIG welding SUN Qingjie[1,2], LI Wenjie[1], HU Haifeng[1], LIANG Yingchun[2], FENG Jicai[1] (1. Shandong Provincial Key Laboratory of Special Weiding Technology, Harbin Institute of Technology at Welhai, Weihai 264209, China; 2. Mechanical Engineering Mobile Postdoctoral Center, Harbin Institute of Technology, Harbin 150001, China). pp 9 - 12

Abstract: The narrow-gap TIG welding with magnetic control system was used to weld the Ti-6Al-4V alloy of 56 mm in thickness. The mechanical properties of weld bead were tested including tensile strength, impact toughness, and hardness. The results shows that the tensile strength value is higher than that of the filler metal due to the meshing strengthened effect. The stress distribution along the through-thickness direction of the joint determines the highest tensile strength and toughness value in the area nearby the welding center line. The welding stress between surface layer and interlayer makes the tensile strength and toughness value decreased. The surface layer has the medium value without welding stress. The highest hardness value appears in the fusion line at the same position on depth because of the acicular α′.

Key words: titanium alloy; narrow-gap welding; magnetic control arc; mechanical properties

High temperature strorage reability of Cu bonds by ultrasonic bonding with fine copper wire HANG Chunjin[1,2], TIAN Yanhong[1], WANG Chunqing[1], ZHAO Jiupeng[2] (1. State Key Laboratory of Advanced Welding and Joining, Harbin Institute of Technology, Harbin 150001, China; 2. School of Chemical Engineering and Technology, Harbin Institute of Technology, Harbin 150001, China). pp 13 - 16

Abstract: The high temperature strorage reliability of Cu bonds formed with 20 μm copper wire by ultrasonic bonding process after encapsulation with epoxy molding compounds was investigated. SEM was used to analyze the interfacial microstructure and IMCs on the bonding interface after thermal aging. EDS was used to identify the IMCs compositions. A great amount of Cu/Al IMCs as well as micro-cracks and Kirkendall voids are found on the bonding interface after thermal aging with 9 days at 200 ℃ and with 9 hours at 250 ℃. With 16 hours aging at 250 ℃, the element Sb which is decomposed from the epoxy molding

compounds started to react with Cu ball bonds to form Cu_3Sb. When the aging time is more than 49 hours at 250 ℃, Cu wire loop is broken and serious corrosion is found in Cu ball bond. Furthermore, Ag migration phenomenon occurs if the aging time is more than 24 hours at 250 ℃ or 4 hours at 300 ℃.

Key words: fine Cu wire; high temperature storage; IMC; reability; Ag migration

An ultrasonic SH-guided-wave transducer for ultrasonic imaging and testing of plate with welded structure ZHU Xinjie, CHEN Yifang, HAN Zandong, DU Dong (Key Laboratory for Advanced Materials Processing Technology, Ministry of Education, Tsinghua University, Beijing 100084, China). pp 17 – 21

Abstract: The SH (shear horizontal) guided waves can be used to test and image in long distance for the larger-sized plate in welded structure. The performance of ultrasonic SH-guided-waves transducer is essential to imaging and testing larger-sized plate in welded structure. The dynamic analysis of SH guided wave in plate and half-wave propagation conditions was carried out. The reasonable wedge angle, the frequency, size of the piezoelectric wafer for SH-guided-waves transducer and other important parameters were designed. The steps such as adding the front lining, removing the back lining, setting the jagged slot on front wedge and so on, have reduced the internal echo interference in SH-guided-waves transducer, which improves the testing sensitivity and simplifies the transducer structure. The results shows that the developed SH-guided-waves transducer has the better testing ability and can be used in imaging and testing complex T-butt type welded structure. The image can characterize the defects, whose size is close to the guided wave length in the welded structure. The proposed research provides the foundation for the imaging and testing of larger-sized plate with welded structure.

Key words: ultrasonic; shear horizontal-guided-wave transducer; welded structure

Effect rule of torch angle change on weld formation of keyhole plasma arc welding JIANG Fan, CHEN Shujun, WANG Long, YU Yang (College of Mechanical Engineering and Applied Electronics Technology, Beijing University of Technology, Beijing 100124, China). pp 22 – 26

Abstract: By taking 5 mm thick 5A06 aluminum-magnesium alloy as the main researching object, the front and back weld width as the formation parameter, the significance of torch angle to weld formation was studied by the orthogonal experiment, the effect of change of torch angle on weld formation was studied from the point of energy transfer. The result shows that the influence of the torch angle on welding formation is between current and plasma gas flow rate. There is largest front weld width when the torch is perpendicular to the test plate. The back weld width will be larger with the torch angle increasing. It indicates the energy density on the front surface, the relative position of the highest temperature section and the widest molten section will be changed by torch angle change. The effect on the back weld width may be caused by the interaction of sectional heat source deviation of different thickness direction and the delay of heat transfer.

Key words: keyhole plasma arc welding; torch travelling angle; weld formation; orthogonal experiment

Statistic analysis on spatter characteristics in high power CO_2 laser and fiber laser welding of thin sheet aluminum alloy CAI Hua, XIAO Rongshi (Institute of Laser Engineering, Beijing University of Technology, Beijing 100124, China). pp 27 – 30

Abstract: Spatters in laser penetration welding of aluminum alloys affects the process stability and reflects the laser welding process to a certain degree. The spatter characteristics in CO_2 laser and fiber welding of 6061-T6 aluminum alloy were investigated, and the reasons for the difference in spatter characteristics were discussed. Dynamic behavior of spatters was recorded in real-time by a high-speed camera. The spatter particles were captured and their sizes were measured experimentally. Probability density functions (PDFs) about the spatter velocity and size were fitted by Ordinary Least Squares (OLS) method in X^2 test. The result indicates that the spatter speed follows Gaussian distribution and the particle size follows lognormal distribution in both cases. However, the statistical speed of spatters is faster in fiber laser welding, which indicates that more attention should be paid to protect the focusing system. Moreover, the statistical diameters of the spatter particles are smaller and PDFs of the particle size is more fit with Lognormal distribution in fiber laser welding, which means that fiber laser welding process is more stable than CO_2 laser welding process.

Key words: thin sheet aluminum alloy; high power laser welding; spatter characterization; statistic analysis

Selection method of X-ray diffraction stress measurement parameters for titanium and titanium alloy DENG Yunhua, LI Xiaoyan, LI Qingqing, LU Wei (School of Materials Science and Engineering, Beijing University of Technology, Beijing 100124, China). pp 31 – 34, 39

Abstract: Considering the low intensity of diffraction peak, bad diffraction profile, wide fluctuation range and low accuracy of the stress measurement results for titanium and titanium alloy, the effects of aperture diameter, exposure time, and exposure number on the intensity of X-ray diffraction peak, net intensity, full width at half maximum, and the stress measurement results were investigated through the X-ray stress measurement of free stress standard sample and high stress standard sample. On this basis, the selection method of X-ray diffraction stress measurement parameters for titanium and titanium alloy was decided and used in measuring the residual stresses in TC4 welded joint. Results show that with the increase of aperture diameter and exposure time, the intensity of X-ray diffraction peak increases, both the diffraction profile and the accuracy of the test results are improved. What's more, with the increase of exposure number, the diffraction profile and the accuracy of the test results are also improved. The measurement results of residual stresses in TC4 welded joint meet the requirements of the related standards.

Key words: titanium alloy; X-ray stress measurement;